JOURNAL OF MATERIALS SCIENCE 27 (1992) 4393–4405

Effect of modulus and cohesive energy on critical fibre length in fibre-reinforced composites

L. MONETTE, M. P. ANDERSON, S. LING, G. S. GREST
Corporate Research Science Laboratory, Exxon Research and Engineering Company, Annandale, NJ 08801, USA

The effect of fibre modulus and cohesive energy on critical fibre length and radius in ceramic-fibre-reinforced brittle composites has been investigated employing both analytical theory and computer simulation. The theory consists of a shear-lag analysis in which an energy failure criterion is incorporated. The simulation consists of a two-dimensional computer model based upon a discrete network of grid points. Failure is also defined in terms of an energy criterion, where the energy is calculated on the basis of a two- and three-body interaction between the grid points. Both theory and simulation show that a minimum critical aspect ratio is found as a function of the elastic moduli ratio, E_f/E_m, with a divergence occurring at both low- and high-modulus values. As the modulus ratio is increased, there is a transition in failure mechanism from tensile-dominated failure in the matrix to shear-dominated failure at the fibre–matrix interface. In addition, families of critical aspect ratio curves are obtained as a function of the cohesive energy ratio, U_f/U_m. Larger cohesive energy ratios shift the critical aspect ratio curve to larger values. These features potentially explain trends in the experimental results reported by Asloun *et al.*, where the critical fibre aspect ratio was measured for fibre/matrix systems having different modulus and toughness ratios.

1. Introduction

Optimum mechanical properties in composite materials depend on the efficiency of stress transfer from the matrix to the fibres. The efficiency of the transfer determines a critical length, l_c [1–5] for the fibre above which it can be loaded to its full capacity, therefore strengthening the material. Below this critical length the loading efficiency of the fibre decreases and the fibre rather acts as a defect in the material. Hence it is very important from a technological point of view to understand how the critical length depends upon the stress transfer to the fibres. Factors which are known to influence the stress transfer are the structure and properties of the matrix, the fibre and the interface. In particular, interface properties are known to be important, because the stresses induced by the differences between the elastic properties of the matrix and the fibres have to be transmitted through the interface. The overall structure and properties of the matrix, fibre and interface can be characterized by an elastic modulus, E_α, a cohesive energy, U_α, and a viscoelastic coefficient, η_α, for each of these three components, namely the matrix (E_m, U_m, η_m), the fibre (E_f, U_f, η_f) and the interface (E_i, U_i, η_i).

The problem of stress transfer to the fibre has been treated analytically by Cox [6] and is now referred to as the shear-lag theory. The shear-lag theory makes use of the following assumptions.

1. Both the fibre and the matrix remain elastic.
2. The interface is infinitesimally thin.
3. There are no strain discontinuities across the interface, i.e. the bond between the matrix and the fibre is perfect.
4. There is no bonding between the matrix and the end faces of the fibre.

Cox's approach has two major drawbacks. The first one is that it does not take properly into account the stress amplification effects near the fibre tips. Finite element analyses [7–10] have shown that the critical length is highly dependent on assumptions made about local stress concentration. Experimental studies [11, 12] suggest that shear-lag analysis underestimates the shear stress concentration at the end of the fibre. Furthermore, these studies also show that state of stress as well as stress concentration depend also on fibre-end geometry. The second drawback is that end face adhesion is not taken into consideration. Of the two limitations, stress amplification effects would seem even more serious than neglecting the adhesion across the end face of the fibre. This is because in many experimental systems (e.g. epoxy/fibreglass), the fibres are usually coated with an adhesive substance and then chopped.

The definition of a critical length, l_c (or critical aspect ratio l_c/d, where d is the fibre diameter), in short fibre composites is somewhat arbitrary. Fig. 1 illustrates the tensile stress along a single fibre embedded in a matrix. L is the length of the fibre, $l_c/2$ is half the

0022–2461

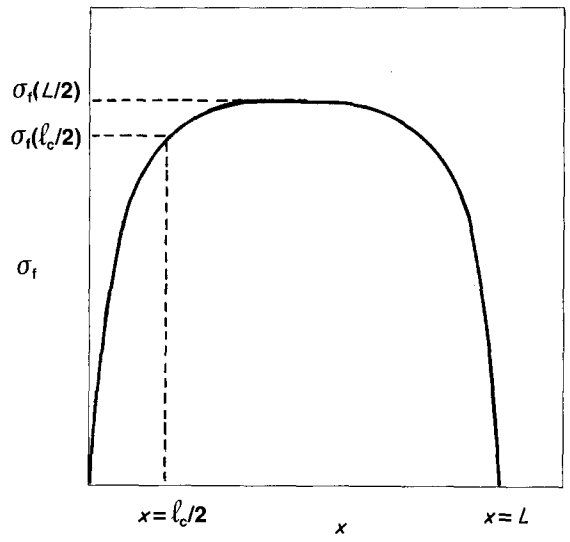

Figure 1 Plot of the tensile stress, σ_f, as a function of the x coordinate along the fibre for a fibre of length L taken from one computer simulation ($L = 27$). The tensile stress at the centre of the fibre, σ_f $(L/2)$ and at half the critical length, σ_f $(l_c/2)$ is illustrated.

critical length (also called the ineffective length), σ_f $(L/2)$ is the stress at the fibre mid-point and $\sigma_f(l_c/2)$ is the fibre stress at a distance $l_c/2$ from the fibre end-point. The critical length is usually defined [2] as the length beyond which the fibre can achieve maximum strain (strain applied to the composite, ε_0) and maximum stress ($\varepsilon_0 E_f$). Another approach is to define the critical length as the distance from the fibre end to the point at which the fibre stress is some specified fraction of the stress in a fibre of infinite length. Rosen [13, 14] used an approach based on the shear-lag theory with a fraction of 0.9 and obtained the following expression for the critical aspect ratio l_c/d:

$$\frac{l_c}{d} = \left(\frac{1}{2}\frac{E_f}{G_m}\frac{1 - v_f^{1/2}}{v_f^{1/2}}\right)^{1/2} \quad (1)$$

where G_m is the shear modulus of the matrix and is equal to $E_m/2(1 + \nu_m)$, ν_m is the Poisson's ratio of the matrix and v_f is the volume fraction of fibres. From the above definitions, one can infer from Equation 1 that the critical aspect ratio is proportional to the square root of the ratio of the elastic moduli, E_f/E_m

$$\frac{l_c}{d} \propto \left(\frac{E_f}{E_m}\right)^{1/2} \quad (2)$$

Galiotis *et al.* [15] obtained a result similar to Equation 2 for the regime $E_f \gg E_m$ by using the shear-lag theory and defining the critical length to be the length at which $\sigma_f(l_c/2) = \sigma_f(L/2)/e$ where e is the natural logarithm. Termonia [16, 17] defined the critical length to be the length at which the fibre strain is 97% of the strain of a fibre of infinite length. Using a finite difference technique which avoids the problems of shear-lag theory concerning stress concentration and end-face adhesion, it was found that

$$\frac{l_c}{d} \propto \frac{E_f}{E_m} \quad (3)$$

i.e. the critical aspect ratio is linearly related to the ratio of the elastic moduli, E_f/E_m. Because the mode of fibre loading assumed by Cox's shear-lag theory and Termonia [16, 17] is not quite the same (pure shear loading versus a mixture of tensile and shear loading), it is not surprising that the functional dependences obtained for the critical length are different. In a recent paper by Asloun *et al.* [18], the critical aspect ratio predicted by the shear-lag theory and Termonia are compared to experimental results for a variety of systems. Most systems seem to agree with the predictions based on the shear-lag theory for large values of the ratio E_f/E_m, while only a few seem to follow Termonia's prediction [16, 17], indicating that indeed stress concentration at the fibre ends is negligible. However, the data also seem to show an upward trend at lower values of the ratio E_f/E_m, in disagreement with both the predictions of Termonia [16, 17] and the shear-lag theory (see Fig. 2). This trend is described by Asloun *et al.* [18] in terms of a scatter of the data, due to variations in adhesion. Asloun *et al.* [18] pointed out that such variations in adhesion are experimentally very difficult to check. Moreover, the data do not collapse on one single curve for $E_f \gg E_m$ but rather on two such distinct curves, corresponding to systems with thermosetting/thermoplastic matrices and to systems with elastomeric matrices respectively. The critical length for elastomeric matrices was found to be about seven times smaller than the critical length for thermosetting or thermoplastic matrices. Therefore, this experimental study concluded that the nature of the matrix plays an unexpected role in stress transfer.

The discrepancies reported by Asloun *et al.* [18] suggest that additional parameters may be needed to describe properly load transfer in short fibre composites. The theoretical approaches reported in the literature [1–6] do not take explicitly into consideration the cohesive energy of the fibre and the matrix, and this factor can indeed modify the functional dependence of the fibre critical length, l_c. This work, therefore, proposes to further our understanding of the nature of stress transfer by studying the critical length as a function of two parameters; namely, the ratio of the elastic moduli, E_f/E_m, and the ratio of the cohesive energies, U_f/U_m. The cohesive energy parameter is brought into this study by generalizing the failure mechanism to incorporate many possible failure modes, i.e. we introduce an energy-failure criterion in the equations of shear-lag theory described and in a computer model described. The simulation results are also presented.

2. Theory

The results from this section will be compared to our two-dimensional computer model, therefore we present those results in three- and two-dimensional form. Let us consider a single fibre of elastic modulus, E_f, radius, r_f, and cohesive energy, U_f, embedded in a soft matrix of elastic modulus, E_m, Poisson's ratio, ν_m, and cohesive energy, U_m, as illustrated in Fig. 3. R is half the interfibre spacing, $\tau(x, r)$ is the shear stress in the

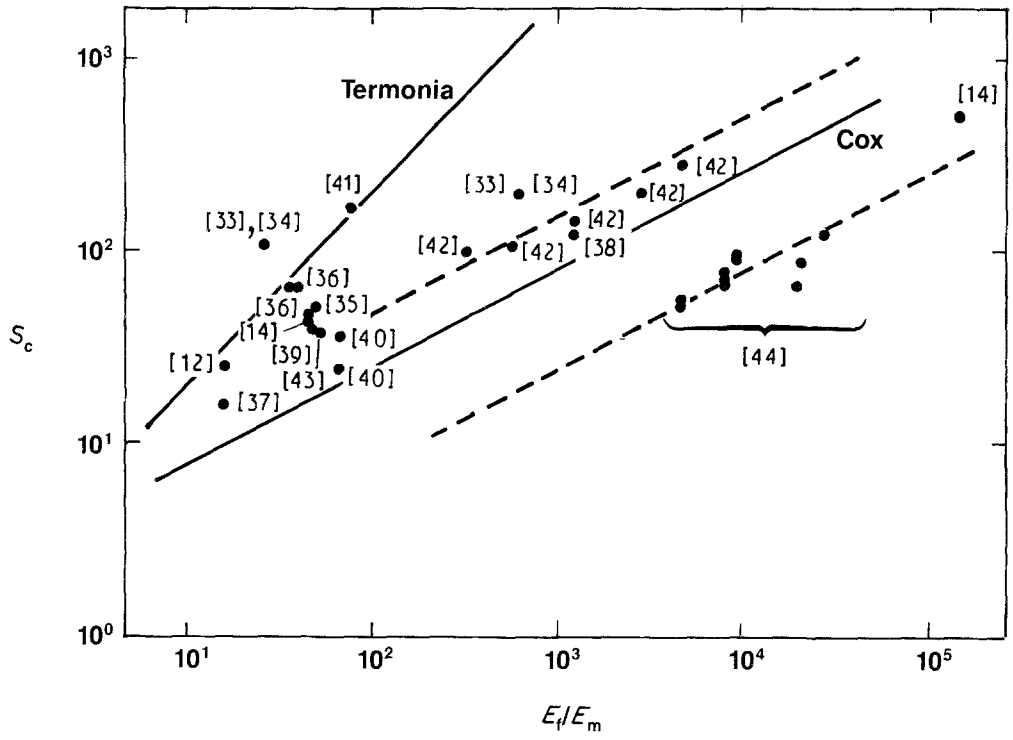

Figure 2 Critical aspect ratio, S_c, as a function of E_f/E_m in logarithmic scale. The data are taken from the literature by Asloun *et al.* [18]. (——) The theoretical prediction of shear-lag theory [3] (Equation 1) and of Termonia [16], (– – –) experimental fittings.

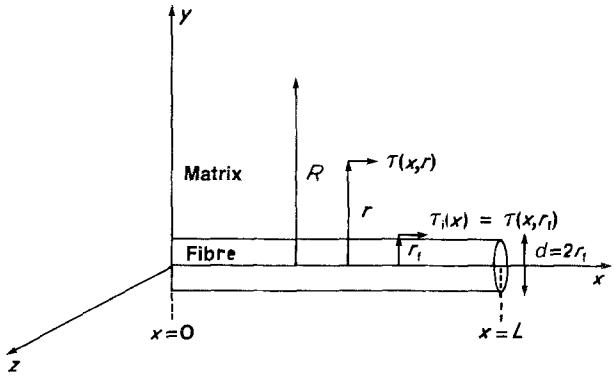

Figure 3 Fibre embedded in the matrix. The fibre has length L, radius r_f. The origin of the coordinate system corresponds to one of the fibre ends and the fibre axis is along the x direction. τ_i is the shear stress at the fibre–matrix interface, τ is the shear stress at a distance $r = (y^2 + z^2)^{1/2}$ (cylindrical symmetry is assumed) and R is a distance large enough so the strain on the matrix beyond the distance R is the same as the applied strain.

matrix a distance $r = (y^2 + z^2)^{1/2}$ (assuming cylindrical symmetry) above a given x coordinate along the fibre, $\tau(x, r_f) = \tau_i(x)$ is the shear stress at a given x coordinate along the fibre–matrix interface and $d = 2r_f$ is the diameter of the fibre. According to Cox's assumptions presented in the previous section, we can balance the shear forces in the matrix $\tau(x, r)$ with the shear forces at the fibre–matrix interface, $\tau_i(x)$. For a three-dimensional system, one obtains $2\pi r_f \tau_i(x)\,dx = 2\pi r\tau(x, r)\,dx$ or $\tau(x, r) = r_f\tau_i(x)/r$. Using $\tau = G_m\gamma_m$, where $\gamma_m = du/dz$ is the shear strain and $u = u(x, r)$ is the displacement we obtain

$$\frac{du(x, r)}{dr} = \frac{\tau(x, r)}{G_m} = \frac{r_f\tau_i(x)}{rG_m} \tag{4}$$

We then proceed to integrate the left-hand side of Equation 4 from $u(x, r_f)$, the fibre displacement to $u(x, R)$, the matrix displacement at a distance, R (see Fig. 3), and the right-hand side of Equation 4 from r_f to R with the result

$$u(x, R) - u(x, r_f) = \frac{r_f\tau_i(x)}{G_m}\ln(R/r_f) \tag{5}$$

and

$$\tau_i(x) = \frac{[u(x, R) - u(x, r_f)]E_m}{2r_f(1 + \nu_m)\ln(R/r_f)} \tag{6}$$

Balancing the shear forces at the interface with the tensile force in the fibre over an element of length dx

$$\frac{d\sigma_f(x)}{dx} = -\frac{2\tau_i(x)}{r_f} \tag{7}$$

in three dimensions, and differentiating with respect to x results in the following expression:

$$\frac{d^2\sigma_f(x)}{dx^2} = \frac{E_m[\sigma_f(x) - \varepsilon_m E_f]}{r_f^2 E_f(1 + \nu_m)\ln(R/r_f)} \tag{8}$$

where $\varepsilon_m = du(x, R)/dx$ and $\varepsilon_f = du(x, r_f)/dx = \sigma_f(x)/E_f$. Note that no stress amplification is possible in the shear-lag approach. The solution to Equation 8, which is the tensile stress along the fibre together with the boundary conditions $\sigma_f(x = 0) = \sigma_f(x = L) = 0$ (boundary condition for a fibre with no end-face adhesion) for a fibre of length, L, is as follows for a three-dimensional system:

$$\sigma_f(x) = \frac{E_f}{E_m}\sigma_m\left[1 - \frac{\cosh\beta(x - L/2)/r_f}{\cosh\beta L/2r_f}\right] \tag{9}$$

and

$$\beta = \left[\frac{E_m}{E_f(1 + \nu_m)\ln(R/r_f)}\right]^{1/2} \quad (10a)$$

In two dimensions, the expression for the tensile stress is the same as given by Equation 9; however

$$\beta = \left[\frac{E_m}{2E_f(1 + \nu_m)(R/r_f - 1)}\right]^{1/2} \quad (10b)$$

The shear stress at the fibre–matrix interface for a three-dimensional system is obtained by using Equations 7 and 9

$$\tau_i(x) = \frac{\beta}{2}\frac{E_f}{E_m}\sigma_m\left[\frac{\sinh\beta(x - L/2)/r_f}{\cosh\beta L/2r_f}\right] \quad (11a)$$

and in two dimensions

$$\tau_i(x) = \beta\frac{E_f}{E_m}\sigma_m\left[\frac{\sinh\beta(x - L/2)/r_f}{\cosh\beta L/2r_f}\right] \quad (11b)$$

This work will make use of the following definition for the critical length, l_c, commonly used experimentally [19–21]: let a system composed of a single fibre embedded in a matrix be strained until the occurrence of catastrophic failure. Failure will be initiated in the fibre if the fibre length $L > l_c$; failure will be initiated in the matrix if the fibre length $L < l_c$ and for a fibre of length $L = l_c$, failure occurs simultaneously in the fibre and in the matrix. We will explicitly incorporate information concerning the failure stress of the fibre (tensile regime: $\sigma_f(x = L/2) = \sigma_f^*$ for $L \geqslant l_c$) and the matrix into the equations of shear-lag theory with two different possible mechanisms of failure in mind for the matrix.

1. Because stress transfer efficiency is not as large as low values of the ratio E_f/E_m, one can expect that tensile stress builds up in the matrix, ultimately causing failure to be initiated in the matrix for a fibre of length $L < l_c$.

2. The stress transfer efficiency increases as the value of E_f/E_m increases. One therefore expects low levels of tensile stress in the matrix, but that the shear stresses generated at the fibre–matrix interface close to the fibre tips are now becoming large, hence should dominate the failure mechanism of a fibre of length $L < l_c$. The important failure parameter for a fibre of length $L < l_c$ is $\tau_i(x = 0) = \tau_i^*$, the shear failure stress of the matrix.

In order to calculate the critical aspect ratio for the first failure condition valid for low values of E_f/E_m, we set the fibre length $L = l_c$. The condition $L = l_c$ enables us to replace simultaneously the stress in the fibre, $\sigma_f(x = L/2)$, and the stress in the matrix, σ_m in Equation 9 by their respective breaking stress, σ_f^* and σ_m^*. In our approach, the failure stress of the fibre and the matrix are energy controlled: $\sigma_f^* = (2E_fU_f)^{1/2}$ and $\sigma_m^* = (2E_mU_m)^{1/2}$ where, for simplicity, we have used an harmonic approximation to obtain the cohesive energies, $U_\alpha = \sigma_\alpha^2/2E_\alpha$. Defining $E = E_f/E_m$ and $U = U_f/U_m$, we obtain the following expression for the critical aspect ratio $S_c = l_c/d$ (where d is the fibre diameter) for an energy controlled failure criterion

$$S_c = \frac{1}{\beta}\cosh^{-1}\left[\frac{E}{E - (UE)^{1/2}}\right] \quad (12)$$

which we will compare to the critical aspect ratio for a stress-controlled failure criterion

$$S_c = \frac{1}{\beta}\cosh^{-1}\left[\frac{E}{E - \sigma_0}\right] \quad (13)$$

where $\sigma_0 = \sigma_f^*/\sigma_m^* = $ constant. Fig. 4a is a plot of Equations 12 and 13. Equation 12 possesses two interesting features. First, an energy failure criterion seems to cause the appearance of a minimum aspect ratio, which is not the case for Equation 9, i.e. in Equation 13 $dS_c/dE|_{E=E_0} \to 0$ only for $E_0 \to \infty$. Furthermore, the critical aspect ratio given by Equation 12 diverges at a low values of E and the asymptote is located at $E = U$ while for $E \to \infty$ it diverges as $E^{1/4}$. The critical aspect ratio given by Equation 13 diverges for $E = \sigma_0$ but remains constant as $E \to \infty$. In addition, an energy failure criterion generates families of curves for different cohesive energy ratios, U, as shown on Fig. 4b, while the stress-controlled failure does not depend on the ratio U.

We have obtained the critical aspect ratio by assuming that pure tensile failure occurred in the matrix ($\sigma_f^* = (2E_mU_m)^{1/2}$). Let us now obtain the critical aspect ratio for the second failure mechanism where failure is dominated by the shear stresses at the fibre–matrix interface close to the fibre tips. We rewrite the shear stress at the fibre end point in terms of the maximum fibre stress $\sigma_f(x = L/2)$ for a fibre of length $l_c = L$ with the help of Equations 9 and 11a

$$\tau_i(x = 0) = \tau_i^* = \frac{\beta}{2}\left[\frac{\sinh\beta S_c}{\cosh\beta S_c - 1}\right]\sigma_f^* \quad (14a)$$

and in two dimensions, with the help of Equation 11b

$$\tau_i(x = 0) = \tau_i^* = \beta\left[\frac{\sinh\beta S_c}{\cosh\beta S_c - 1}\right]\sigma_f^* \quad (14b)$$

We substitute the following two expressions for the failure parameters of the matrix and the fibre into Equation 14a for a three-dimensional system: $\tau_i^* = (2G_mU_m)^{1/2}$, but σ_f^* is still given by $(2E_fU_f)^{1/2}$ and we obtain, after a few manipulations

$$S_c = \frac{1}{\beta}\cosh^{-1}\left[\frac{C + 1}{C - 1}\right] \quad (15)$$

In three dimensions β in Equation 15 is given by Equation 10a and

$$C = 2\frac{\ln(R/r_f)}{U} \quad (16a)$$

In two dimensions, β in Equation 15 is given by Equation 10b and

$$C = \frac{(R/r_f - 1)}{U} \neq 1 \quad (16b)$$

Note that $C \neq 1$ because $\ln(R/r_f)$ or $R/r_f \gg 1$ in the dilute limit and $U > 1$. Fig. 4c is a plot of Equation 15

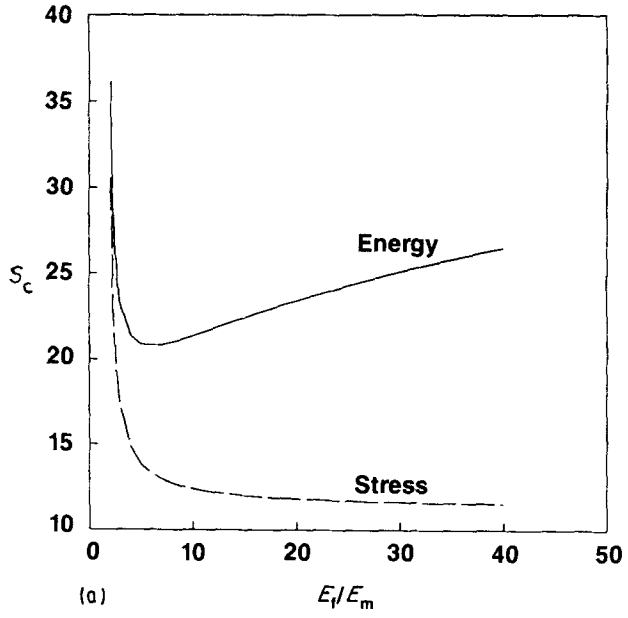

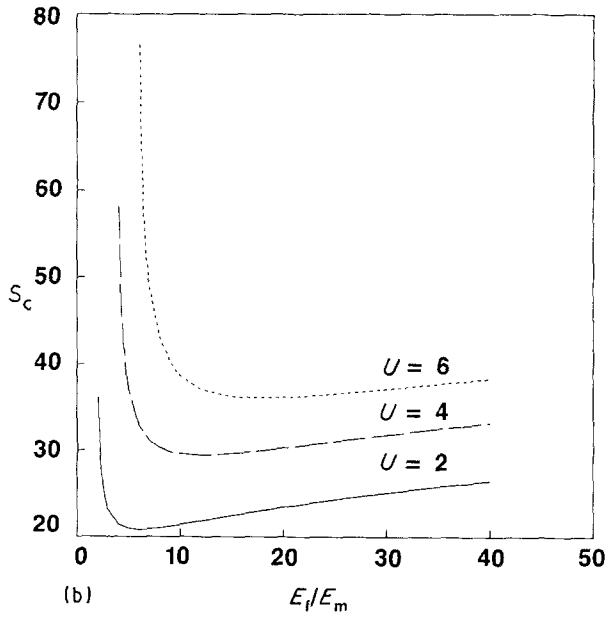

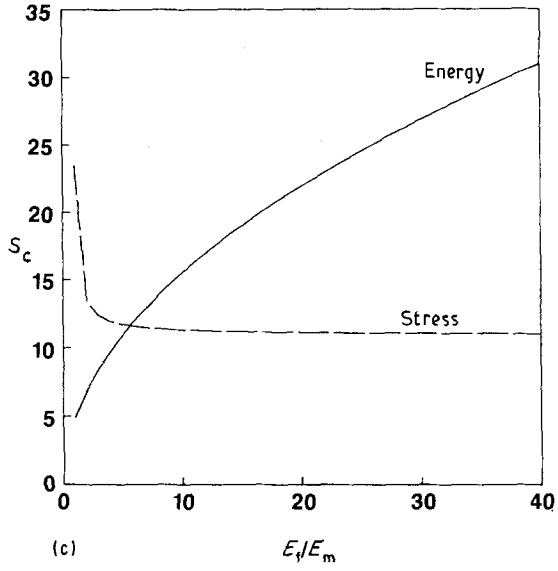

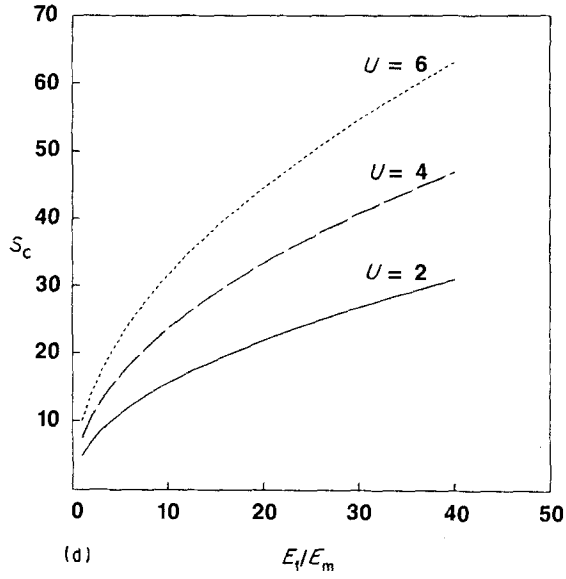

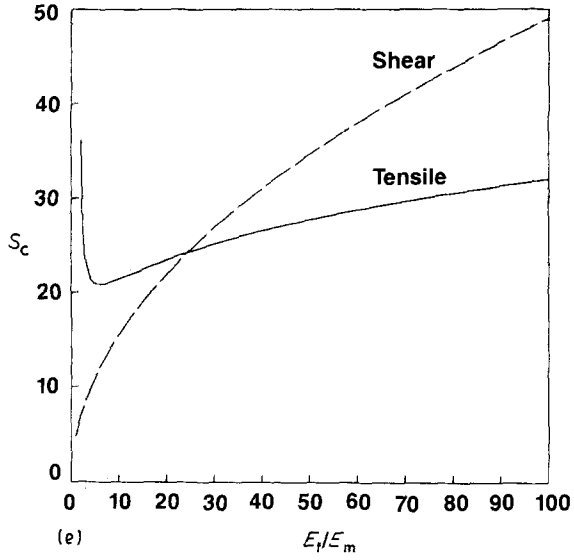

Figure 4 (a) Plot of the critical aspect ratio S_c as a function of $E = E_f/E_m$. (——) An energy-controlled failure criterion (tensile dominated regime), (– – –) a tensile stress failure criterion. (b) Plot of families of critical aspect ratio curves as a function of $E = E_f/E_m$ in the case of an energy-controlled failure criterion (tensile dominated regime) for three values of the parameter $U = U_f/U_m = 2$ (——), 4 (– – –) and 6 (. . . .). (c) Plot of the critical aspect ratio, S_c, as a function of $E = E_f/E_m$. (——) An energy-controlled failure criterion (shear dominated regime), (– – –) a shear stress failure criterion. (d) Plot of families of critical aspect ratio curves as a function of $E = E_f/E_m$ in the case of an energy-controlled failure criterion (shear dominated regime) for three values of the parameter $U = U_f/U_m = 2$ (——), 4 (– – –) and 6 (. . .). (e) Plot of the critical aspect ratio, S_c, for an energy controlled failure criterion. (——) The tensile-dominated regime, (– – –) the shear-dominated regime. The overall behaviour of S_c is obtained by deleting the lower branches (see Fig. 6c).

for the critical aspect ratio using an energy-controlled failure criterion. This is compared to the critical aspect ratio obtained from a stress-controlled failure mechanism $\tau^* = \text{const}$ and $\sigma^* = \text{const}$ where S_c is given by Equation 15 with

$$C = \left(\frac{\tau^*}{\sigma^*\beta}\right)^2 \tag{17}$$

Here again β is given by Equations 10a and b for three and two dimensions, respectively. The functional dependence of S_c in Equation 15 with respect to E for E

large, is

$$S_c \sim E^{1/2} = \left(\frac{E_f}{E_m}\right)^{1/2} \quad (18)$$

for an energy-controlled failure criterion in two and three dimensions, while for a tensile stress controlled criterion τ_i^*/σ_f^* is a constant (Equation 15 together with Equation 17) gives $S_c \to$ constant as E increases. The critical aspect ratio decreases monotonically with the ratio of elastic moduli, E, in the case of a stress-controlled failure criterion (Equations 13 and 15 with Equation 17), because the expression for the stress in the fibre (Equation 9) predicted by shear-lag theory is an increasing function of E. The case of a tensile stress failure criterion is similar to the behaviour found for the critical aspect ratio when a tensile stress failure criterion (σ_f^*/σ_m^* is a constant) was used (Equation 13). This similarity in behaviour makes sense intuitively: shear-lag theory predicts that the load-transfer efficiency increases with E, the elastic modulus ratio and in the absence of stress concentration, as the stress required to break the fibre or the matrix bonds remains constant as E increases, the critical length must consequently decrease. Fig. 4d illustrates families of curves obtained for an energy-controlled failure criterion using different ratios of cohesive energies, namely $U = 2$, 4 and 6. Fig. 4e illustrates the results obtained for an energy-controlled failure criterion with $U = 2$ when the two failure mechanisms for the matrix envisioned in this work are considered, i.e. the critical length obtained when tensile failure occurs simultaneously in the matrix and in the fibre (Equation 12) together with the critical length obtained when shear failure in the matrix occurs simultaneously with tensile failure in the fibre (Equation 15). The behaviour of the critical aspect ratio over the entire range of E_f/E_m is obtained by selecting the upper branches of the tensile and shear failure curves in Fig. 4e. An example of the resulting theoretical curve for the critical aspect ratio is shown later in Fig. 6c.

Note that the dimensionality introduces an amplitude difference (factor 1/2) in the expressions for $\tau_i(x)$, and β, but does not alter the functional dependence of the critical length on E or U.

3. The model

In order to examine the validity of the above theoretical development in well-controlled ideal conditions, we resort to the use of computer simulations. The ultimate goal is to provide an understanding of the factors which influence the critical length in multi-fibre composites, hence the need to consider factors such as the volume fraction of fibre, interface characteristics and viscoelastic effect, among others. As a first step, we consider the dilute limit, i.e. one single fibre of thickness unity embedded in the matrix. The viscoelastic effects are neglected, which implies that the time scale over which the material is strained is short enough so the behaviour of the material is brittle (i.e. η_m, η_f and $\eta_i = \infty$). This is certainly the case for epoxy/fibre glass system, for which much experimental data is available [5]. In order to simplify the model further, we approximate the non-linear stress/strain behaviour found in real systems by a linear elastic behaviour, which is not expected to change the qualitative trend of the results obtained. The interface considered is as simple and perfect as possible and possesses an elastic constant and a cohesive energy equal to those of the matrix.

The model [22, 23] is not a microscopic, but rather a coarse-grained (i.e. continuum) spring model on a two-dimensional triangular lattice. The hamiltonian contains the usual two-body term, $E_\alpha(r_{ij} - r_0)^2$ as well as a three-body term, $c(\cos\theta_{ijk} - \cos\theta_0)^2$.

$$H = \frac{1}{2}E_\alpha \sum_{ij}(r_{ij} - r_0)^2 + \frac{1}{2}c\sum_{ijk}(\cos\theta_{ijk} - \cos\theta_0)^2 \quad (19)$$

where α = m (matrix), f (fibre) or i (interface), $r_0 = 1$ and $\theta_0 = \pi/3$ are the equilibrium bond length and angle, and θ_{ijk} is the angle between two adjacent bonds (i–j and i–k). The three-body term ensures stability of the model with respect to shear and the three-body constant, c, is taken to be the same for the matrix, and the interface. In most of this paper, we choose $c = E_m/7$, which yields a Poisson's ratio $\nu = 0.1$. Polymer matrices usually have a Poisson's ratio close to 0.3, while glass has a Poisson's ratio close to 0.2. Because the fibre considered in the simulations is dimensionless, i.e. it consists of a single line of nodes, we assume it has a null Poisson's ratio. We must therefore give the matrix a Poisson's ratio of 0.1 in order to achieve the same relative Poisson's ratio $\nu_f - \nu_m$ found in real systems (for instance, glass/epoxy). Results for other values of the matrix Poisson's ratio will be briefly discussed. The stresses generated by the above described model are consistent with the stresses generated by a boundary element analysis [24]. Periodic boundary conditions are applied in the direction of tensile strain (x-axis) while free boundary conditions are applied in the direction perpendicular to the tensile strain (y-axis). The important feature in this work is the fracture criterion in which a bond is broken only if it accumulated an energy greater than its cohesive energy. The advantage of an energy criterion is that it does not restrict the failure mechanism strictly to pure tensile (or pure shear) failure [25]. The failure process is triggered by a combination of shear and tensile stresses, and this combination of stresses defines a fracture surface in stress space [5]. The failure mechanism is therefore allowed to vary continuously with the ratio E_f/E_m from a tensile stress failure regime, where the contribution of the tensile stress term to the energy is dominant to a shear stress failure regime, where the contribution of the shear stress term to the energy is dominant. An energy failure criterion is not artificial nor arbitrary, it is a generalized criterion for failure which encompasses the widely used stress criterion [4, 5, 26] and allows the two failure modes to compete against each other as the ratio of the elastic moduli E_f/E_m is varied. Moreover, recent work [27] reinterpreting fibre pull-out experiments seems to suggest that failure of the

interface between the matrix and the fibre is energy controlled.

The algorithm utilizes a conjugate gradient method to relax the system to its minimal energy configuration and is therefore completely deterministic. The model possesses one more advantage: because of its coarse-grained nature, it allows one to study the onset of fracture from a macroscopic point of view, and therefore should be very useful in studying crack propagation in materials.

4. Simulation results

The critical length is measured using our model in the following way: a fibre of length l is placed at the centre of the triangular lattice and the system matrix(lattice)/fibre is strained until catastrophic failure occurs. If the failure is initiated in the matrix, a new fibre of length $l' > l$ is placed at the centre of the lattice and the experiment is repeated until failure is initiated in the fibre. At this point the length of the fibre is reduced and the experiment is repeated so as to narrow down the critical length between lengths l and $l + 1$ such that for a fibre length of l, failure is initiated in the matrix and for a fibre length of $l + 1$ failure is initiated in the fibre as illustrated in Fig. 5. The critical length l_c is given by $l \pm 1$. In our computer simulations, it is observed that the matrix bonds at the fibre ends always break well before catastrophic failure occurs.

Because periodic boundary conditions are applied in the direction of tensile strain (x direction), one could expect finite size effects to play a significant role especially at large values of the ratio E_f/E_m where the stress and strain amplification at the fibre tips is large. Also, it is intuitively obvious that the loading properties of a system consisting of a fibre embedded in a matrix depend on the quantity of matrix on either side of the fibre. For the sake of meaningful comparisons, critical length measurements were done in the dilute limit, that is for systems with linear dimensions L_x and L_y large (typically $L_x = 300$ and $L_y = 50$) so that increasing the lattice dimensions any further does not have any noticeable effect on the measured critical lengths. The values of E_f/E_m lie between

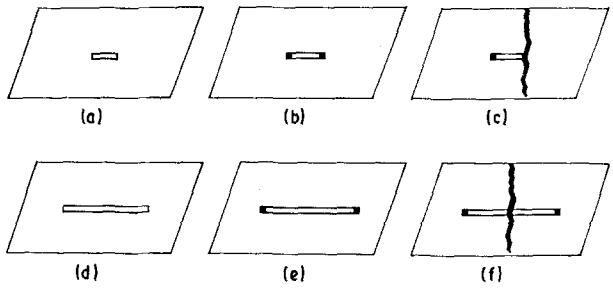

Figure 5 Illustration of the fracture morphology of a sub-critical fibre (a, b and c) and of a super-critical fibre (d, e and f). (a, d) The initial state of the system, i.e. when no strain is applied. (b, e) The system at some intermediate time, when the strain applied causes the bonds at the fibre ends to break. (c, f) The system at catastrophic failure.

$2 < E_f/E_m < 100$ which spans the range of both polymer and ceramic fibres [5, 28, 29]. For computational reasons, the values chosen for U_f/U_m do not necessarily represent real systems. The elastic constants E_α and the cohesive energies U_α are in units of GPa.

Fig. 6a represents a linear plot of the measured critical length l_c versus the elastic moduli ratio E_f/E_m for three different cohesive energies of the fibre, namely $U_f = 0.003, 0.004$ and 0.005. The matrix elastic constant E_m and cohesive energy U_m are kept at a value of 4.5 and 0.002, respectively, throughout this work. Measurements of critical aspect ratio with our model seem to confirm the presence of a minimum aspect ratio. We also show in the inset of Fig. 6a data for a fibre of thickness $d = 3$ as a check that this effect is not an artefact of a fibre of thickness unity. Fig. 6b is a log–log plot of the data in Fig. 6a for $E_f \gg E_m$. The measured slope is close to unity, in agreement with Termonia's results [16] and indicates that the critical aspect ratio varies linearly with the ratio E_f/E_m. Fig. 6c is a plot of our results superimposed with both Equations 12 and 15 in two dimensions. We would like to point out that the expression R/r_f in Equations 12 and 15 was taken as a free parameter in this work in order to fit the data. The distance R is usually taken as half the fibre interspacing in multi-fibre composites, and it is assumed that R is the distance at which the strain in the matrix can be equated with the average tensile strain of the composite. The distance R is probably not a constant, but a function of the elastic moduli ratio and the cohesive energy. For simplicity, we assumed that $R = R(U)$ only in order to fit the data on Fig. 6c. The qualitative agreement of our data with the predicted aspect ratio is good: S_c diverges for both small and large values of E_f/E_m. The upturn in the critical aspect ratio curve occurs at larger values of E_f/E_m as the ratio of cohesive energies is increased, consistent with the predicted asymptote value $E = U$. The value of the minimum aspect ratio increases as well as the value of $E = E_0$ at which this minimum aspect ratio occurs for increasing values of the cohesive energy ratio U (compare also Fig. 6a with Fig. 4b). Our data seems to agree better with the shear failure condition, Equation 15, than with the tensile failure condition, Equation 12, for $E_f \gg E_m$. However, the overall quantitative agreement is poor: S_c varies as $E^{1/2}$ in Equation 15 but in our computer model S_c varies as E. This is to be expected considering the fact that Equation 15 is obtained from a shear failure mechanism of the interface in the proximity of fibre ends together with the inability of shear-lag theory to predict correctly shear stresses at the fibre tips. However, if the function $R(E, U)$ is taken to be approximately constant for $E < E_0$ and to vary as $E^{1/2}$ for $E > E_0$ then the critical length obtained from Equation 15 varies as E, in agreement with the model. Also, excellent quantitative agreement should not be expected for low values [30] of E and many researchers have attributed this discrepancy to the neglect of stress transfer normal to the fibre ends. However, this discrepancy could also be due to the fact that as $E_f \to E_m$, the assumption by shear-lag theory of a negligible tensile stress level in the matrix breaks down. This

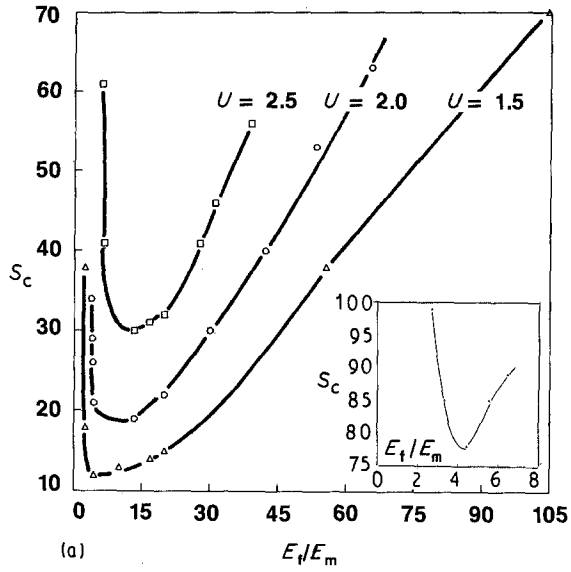

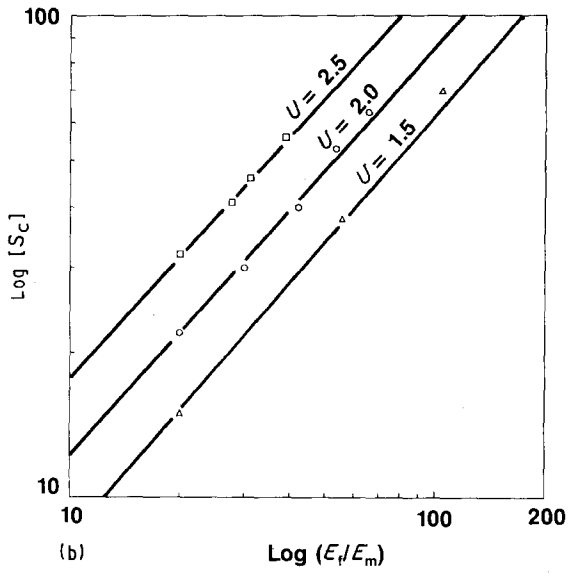

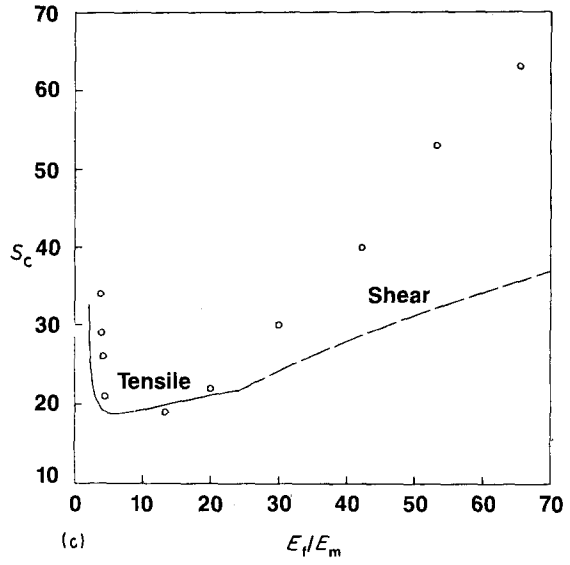

Figure 6 (a) Plot of the computer model results for the critical aspect ratio S_c versus $E = E_f/E_m$ for $U = U_f/U_m = 1.5$ (△), 2 (○) and 2.5 (□). The lines have been added to help the eye and do not represent any fit to the data. The insert at the bottom right represents the critical aspect ratio for a fibre of diameter $d = 2a_0 = 3^{1/2}$ as a function of $E = E_f/E_m$, and $a_0 = 3^{1/2}/2$ is a unit length in the y direction. Note that the y-axis scale of the insert is in units of $1/a_0$. (b) Log–log plot of the critical aspect ratio for $U = U_f/U_m = 1.5$ (△), 2 (○) and 2.5 (□) for values of E greater than 15. The lines do not represent any fit to the data. (c) Plot of the computer results for the critical aspect ratio versus $E = E_f/E_m$ together with the theoretical prediction in case of (——) a tensile-dominated regime and (– – –) a shear-dominated regime for $U = U_f/U_m = 2$. Note that R has been taken as a free parameter to fit the data.

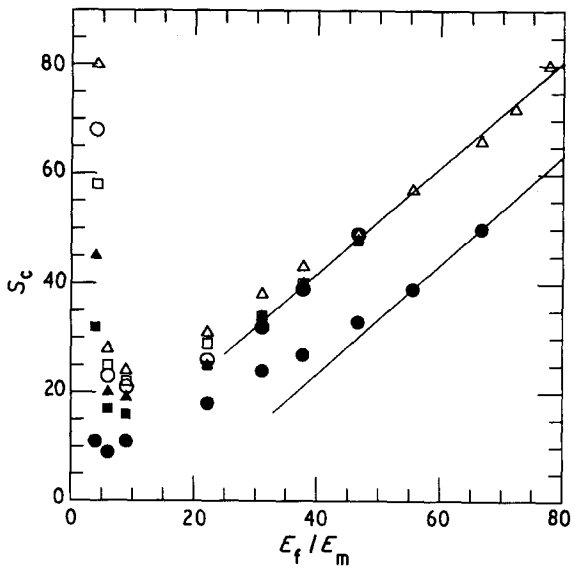

Figure 7 Plot of the critical aspect ratio as a function of the fibre–matrix modulus ratio E_f/E_m for various values of the matrix Poisson's ratio $\nu_m = 0.1428$ (△), 0.1228 (□), 0.1 (○), 0.0667 (▲), 0.0256 (■) and −0.2381 (●).

assumption obviously should be valid only for large values of E. Also, as $E_f \to E_m$, the assumption of small displacements might break down. This assumption is implicitly present in the theory of elasticity and causes the expression for the stress transfer (i.e. Equations 6 and 7) to be a linear function of the displacement difference $u(x, R) - u(x, r_f)$. We plotted in Fig. 7 the critical aspect ratio for different values of the matrix Poisson's ratio. The results clearly show a strong dependence of the critical aspect ratio on the Poisson's ratio difference between the fibre and the matrix, especially at low values of the fibre–matrix modulus ratio, E_f/E_m. However, the dependence of the critical aspect ratio, namely $S_c \sim E_f/E_m$ as E_f/E_m increases ∞ is found to be independent of the matrix Poisson's ratio.

The minimum encountered in Fig. 6a is attributed to two competing factors: the increased efficiency of load transfer to the fibre versus an increase in the shear stresses generated near the fibre ends as the elastic modulus of the fibre is increased. In other words, we have increased the load shed from the matrix to the fibre but we have also increased the shear stress generated on the bonds forming the interface near the fibre ends, i.e. the shear stress on the matrix bonds at the fibre–matrix interface. As this stress becomes large, shear failure occurs prematurely in those bonds, before the fibre can be loaded to its failure point.

Fig. 8a shows the composite stress and strain, as well as the average fibre strain, at the composite failure point. All fibres have the same length, $L = 27$. These three quantities are monotonically decreasing with increasing elastic modulus ratio. This is a consequence of the fact that in the simulations, the toughness (cohesive energy) of the fibre (and not its strength), is kept constant. Therefore, the fibre average strain $\bar{\varepsilon}_f = (2U_f/E_f)^{1/2}$ decreases as the fibre elastic modulus, E_f (or equivalently the elastic modulus ratio), is increased, so that the material is increasingly brittle.

Fig. 8b shows the composite stress at a fixed composite strain ($\varepsilon_0 = 1.42\%$) as a function of elastic modulus ratio. As can be seen, the stress increases non-linearly with elastic modulus ratio. This is due to the fact that the fibre is carrying a larger stress as the elastic modulus ratio increases. The slight non-linearity is a departure from the linear dependence predicted by the rule of mixtures [2, 4, 5], and can be attributed to the change in load-transfer efficiency with modulus ratio.

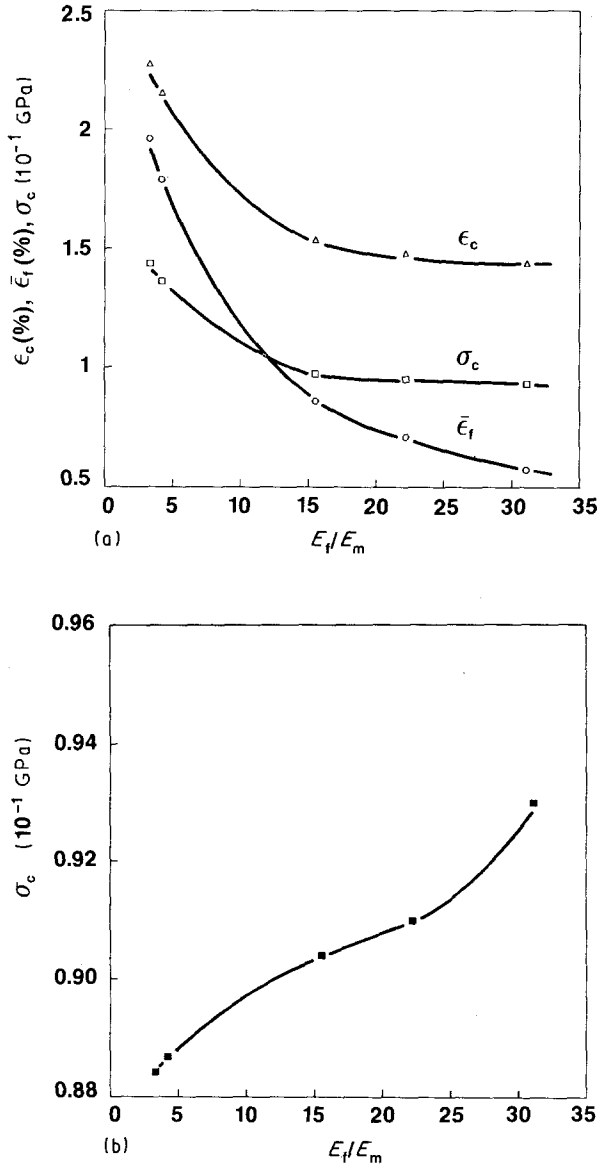

Figure 8 (a) Plot of the composite strain, ε_c (△), the composite stress σ_c (□) and the fibre average strain $\bar{\varepsilon}_f$ (○), as a function of $E = E_f/E_m$. All fibres have length $L = 27$ lattice constants. The solid lines do not represent a fit to the data. (b) Plot of the composite stress, σ_c, at constant composite strain, $\varepsilon_c = 1.42\%$, as a function of $E = E_f/E_m$ for fibres of length $L = 27$ lattice constants. The solid line does not represent a fit to the data.

The tensile stress, σ_i^{xx}, at a site i defined as

$$\sigma_i^{xx} = \sum_{j \in nbh(i)} F_{ij}^x (x_j - x_i) \tag{20}$$

where j is one of the six neighbours of site i and F_{ij}^x is the x-component of the force on i from j, is plotted versus the x-coordinate of the lattice site along the fibre in Fig. 9a. The tensile stress, σ_i^{xx}, at site i is plotted versus the x-coordinate of the lattice sites along the row right below the fibre in Fig. 9b. The shear stress, $\sigma_i^{yx} = \sigma_i^{xy}$, at site i defined as

$$\sigma_i^{yx} = \sum_{j \in nbh(i)} F_{ij}^y (x_j - x_i) \tag{21}$$

where F_{ij}^y is the y-component of the force on i from j, is plotted versus the x-coordinate of the lattice sites along the row below the fibre in Fig. 9c. The x-coordinates on Fig. 9a have been labelled as follows. The ten first sites on the row along the fibre and labelled 1–10 represent the matrix sites to the left of the fibre, the next 27 sites, labelled 11–37, represent the fibre itself and the last 10 sites, labelled 38–47, represent matrix sites to the right of the fibre. The x-coordinates on Fig. 9b and c are labelled 1–47, and represent matrix sites in the row below the fibre. The data on Fig. 9a–c are for fibres of elastic modulus $E_f = 15$, 70 and 140, and cohesive energy $U_f = 0.004$. The length of the fibres is kept constant, $L = 27$, and is sub-critical for $E_f = 15$ and 140, while it is super-critical for $E_f = 70$. One should note that the stress measurements in Fig. 9a–c were taken just before the occurrence of catastrophic failure of the composite and that the stress at a given site, which involves a sum over the site neighbouring bonds should not be confused with the stress in a single bond.

We make the following observations from Fig. 9a.

1. The fibre load increases with increasing fibre elastic modulus (or elastic modulus ratio) which indicates that the fibre is stronger as its elastic modulus is increased. This is consistent with allowing a bond to break according to a constant fibre cohesive energy, rather than according to a constant (tensile or shear) failure stress.

2. The stress level in the matrix on each side of the fibre decreases as the fibre elastic modulus is increased, in agreement with the observed decreasing composite strain at failure of the composite. This is again consistent with breaking bonds according to a constant fibre cohesive energy.

Fig. 9b yields the following observations.

1. Again, the stress level in the matrix to the right and left of the fibre is decreased as the fibre elastic modulus is increased but in addition, one can observe large stress amplification at the sites below (sites 11 and 38) and above (by symmetry; sites 10 and 37) the fibre-end points. Such stress concentration is not taken into account by shear-lag theory.

2. The stress level at those sites is a mixture of stress from bonds stretched in tensile (i.e. b1–b4 in Fig. 10) and in shear (i.e. b5–b8 in Fig. 10) and is about the

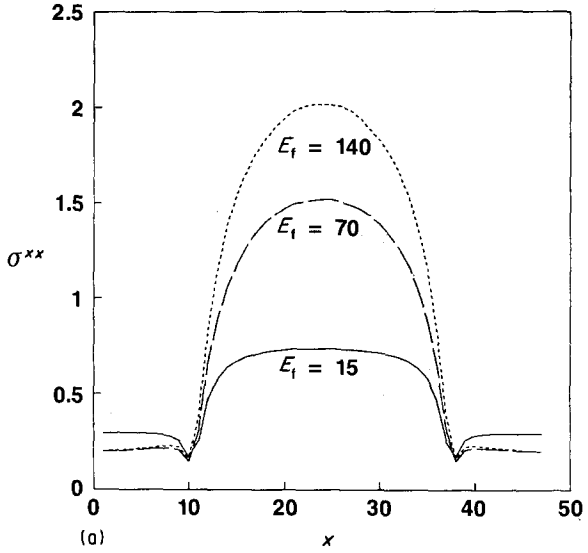

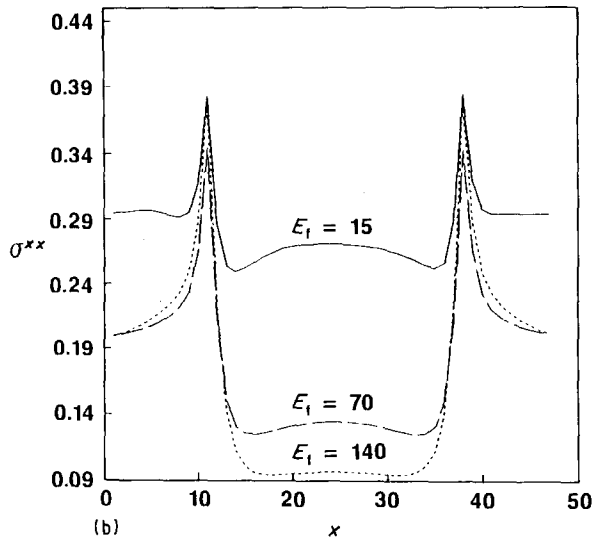

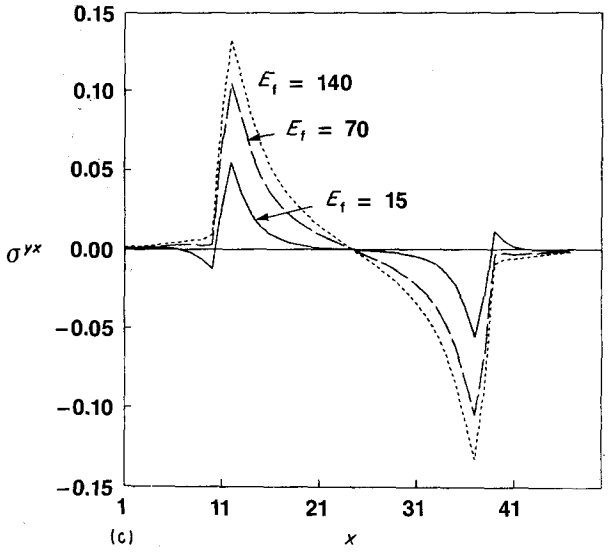

Figure 9 (a) Plot of the tensile stress along the fibre versus the x coordinate of the lattice sites along the fibre. Coordinates 1–10 represents the 10 matrix sites to the left of the fibre. Coordinates 11–37 represents the fibre sites, and coordinates 38–47 represent the 10 matrix sites to the right of the fibre (see also Fig. 10 and caption). The data are taken for fibres of length $L = 27$ and elastic modulus $E_f = 15$ (——), 70 (– – –) and 140 (. . .) for a cohesive energy ratio $U = 2$. The units of stress are $1/2N$ GPa where N is the total number of sites. (b) Plot of the tensile stress along the row of matrix sites below the fibre. Coordinates 1–47 represent matrix sites below the fibre (see also Fig. 10 and caption). (c) Plot of the shear stress along the row of matrix sites below the fibre.

same for all three systems shown on Fig. 9b because those systems are close to failure.

3. The stress in the matrix above and below the fibre is reduced as the fibre elastic modulus is increased, indicating better load transfer with increasing elastic modulus ratio.

Fig. 9c shows clearly that the shear stresses at sites 11 and 38 increase as the fibre elastic modulus ratio increases.

The data provide an understanding of the nature of the transition of failure mechanism by explaining why the fibre length, $L = 27$, is sub-critical for $E_f = 15$, super-critical for $E_f = 70$ and becomes sub-critical again for $E_f = 140$ in spite of increasingly better load transfer to the fibre. This is because a constant fibre

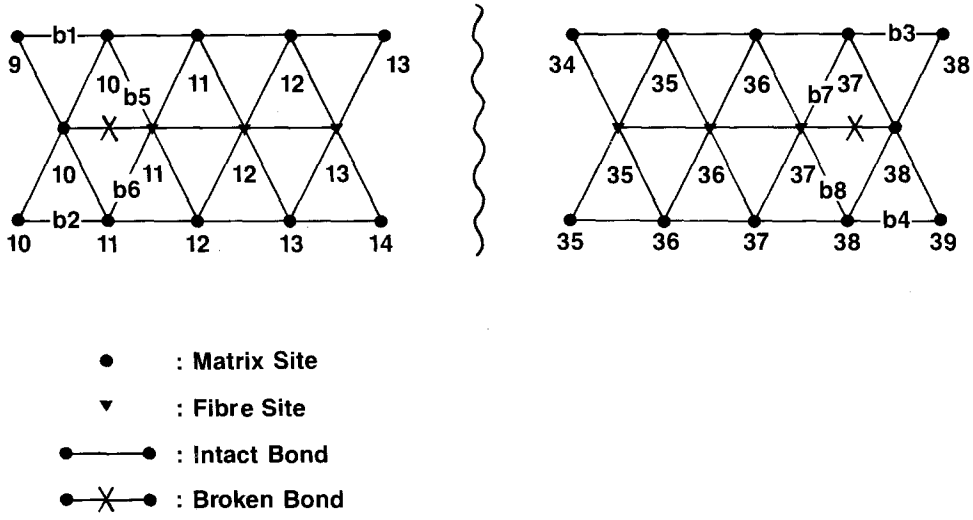

Figure 10 Schematic illustration of the fibre tips (the three first and the three last sites) as well as the rows of matrix sites immediately above and below the fibre. The numbers represent the labels given to the x coordinate of the sites described in Fig. 9. Bonds b1, b2, b3 and b4 are stretched in tensile while bonds b5, b6, b7 and b8 are stretched in shear. A cross on a bond indicates the bond is already broken. The wiggly line indicates that the central part of the fibre (remaining 21 sites for a fibre of length $L = 27$) and the matrix sites above and below are missing.

cohesive energy implies that the stress at failure increases with the fibre elastic modulus, E_f. Moreover, at low elastic modulus ratio, the failure mechanism is dominated by tensile stress amplification: the contribution of bonds b1–b4 (see Fig. 10) to the tensile stress level at sites 11 and 38 shown in Fig. 9b is dominant. This is consistent with the fact the tensile stress in the matrix itself is already high. At higher elastic modulus ratio, the tensile stress level in the matrix is low, because as we pointed out earlier, the composite strain is decreasing. From Fig. 9c one can infer that the failure mechanism is dominated by shear stress amplification: the tensile stress level at sites 11 and 38 no longer come from bonds b1–b4, but must come from the bonds stretched in shear, i.e. b5–b8 on Fig. 10. The minimum seen in Fig. 6a is the boundary between the two failure regimes. This cross-over from a tensile-regime failure to a shear-regime failure is also seen in the fracture of brittle materials with random defects [25] as the defect density increases.

Because the above measurements presented in Fig. 9a–c are made close to the failure point of the composite, i.e. at different composite strains for different values of fibre elastic moduli we show, for purposes of comparison, the tensile stress along the fibre (Fig. 11a), the tensile stress along the row below the fibre (Fig. 11b) and the shear stress along the row below the fibre (Fig. 11c) again for fibres of elastic modulus $E_f = 15$, 70 and 140 and length $L = 27$ at constant composite strain $\varepsilon_0 = 1.42\%$. The same general behaviour and trends as discussed above for Fig. 9a–c are found, but are more pronounced: the load shed to the fibre, the tensile and shear stress concentration at constant composite strain are now far greater for the stiffer fibre, $E_f = 140$, when compared to the softer fibres, $E_f = 15$ and 70.

5. Discussion and conclusion

We studied the load transfer in short fibre composites in the dilute limit as a function of the ratio of the elastic modulus of the fibre to the matrix $E = E_f/E_m$ and as a function of the ratio of the cohesive energy of the fibre to the matrix $U = U_f/U_m$ via an energy criterion for failure. We performed computer simulations on systems consisting of a single fibre of thickness unity in a matrix (dilute limit) in the elastic brittle regime. A minimum critical aspect ratio was found, which appears to be a function of the cohesive energy ratio, U. The minimum critical aspect ratio found is attributed to a compromise between a greater efficiency in load transfer to the fibre as E increases and the amplitude of the shear stresses generated at the fibre ends which causes the matrix to break prematurely. A qualitative theoretical account for this effect was found in terms of equations for tensile and shear stresses given by the shear-lag theory. The functional dependence of the critical aspect ratio is obtained separately for low values of E by balancing a tensile failure criterion for the fibre with a tensile failure criterion for the matrix and for large values of E by balancing the same failure criterion for the fibre with a shear failure criterion for the matrix. In spite of the

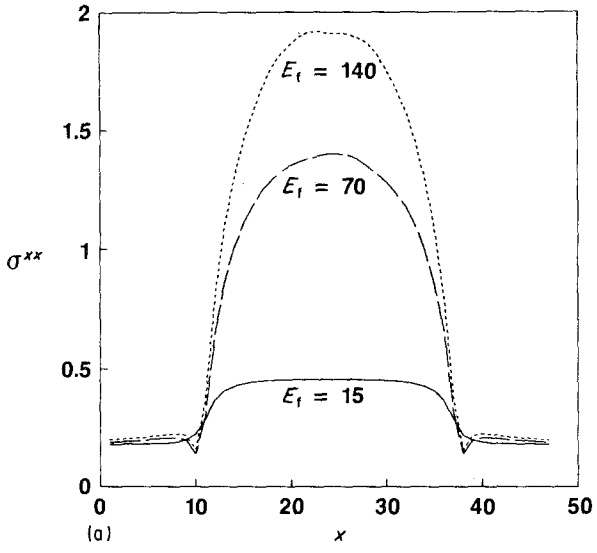

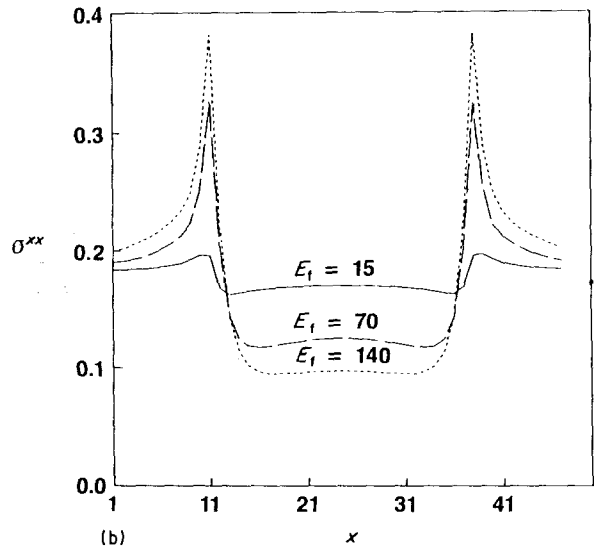

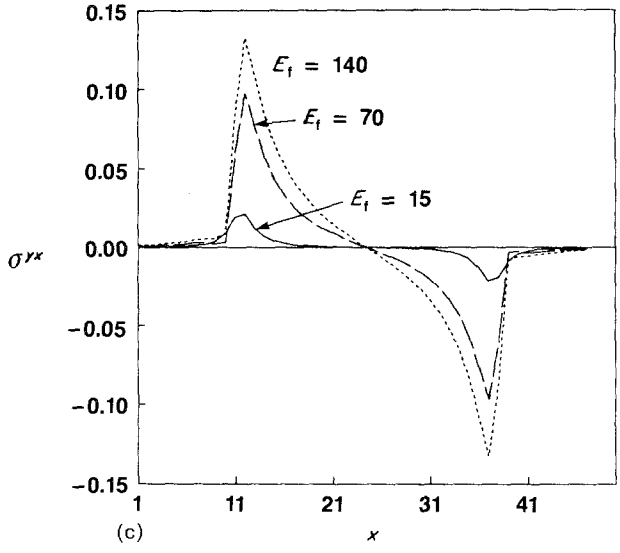

Figure 11 (a) Plot of the tensile stress along the fibre at a constant composite strain $\varepsilon_c = 1.42\%$. See caption for Fig. 9 above. (b) Plot of the tensile stress along the row of matrix sites below the fibre at constant composite strain $\varepsilon_c = 1.42\%$. See caption for Fig. 9 above. (c) Plot of the shear stress along the row of matrix sites below the fibre at constant composite strain, $\varepsilon_c = 1.42\%$. See caption for Fig. 9 above.

good qualitative agreement found, the poor quantitative agreement found between the predicted values of critical aspect ratio from the shear lag theory and the results of the model is not surprising, considering the assumptions of shear-lag theory compared to the computer model. Shear-lag theory does not account for stress concentration at the fibre tips and does not predict the shear stress amplitude correctly. This is obviously not the case in the computer model where large stress concentration can be seen at the fibre-end points. Also, the theoretical expression for the critical aspect ratio obtained in shear-lag theory is derived for two extreme cases of matrix failure:

1. pure tensile failure criterion $U_m = \sigma_m^2/2E_m$, and
2. pure shear failure criterion $U_m = \tau_i^2/2G_m$.

In the model, we expect Case 1 to be valid for values of E close to unity, and Case 2 to be valid for large values of E. However, for intermediate values of E, neither Case 1 nor Case 2 is expected to apply, as the energy in a matrix bond at the fibre–matrix interface is given by $U_m = [A(\sigma_m^2/2E_m)] + [B(\tau_i^2/2G_m)]$, where the exact value of the weights A and B is not known. Presumably, for those intermediate values of E, $A \simeq B$, while Case 1 is for $A \gg B$ and Case 2 is for $A \ll B$.

The divergence in the critical aspect ratio at $E = U$ found in this work can be explained in physical terms. A fibre of elastic modulus $E_f = E_m U$ will reach its breaking energy together with the matrix only for a fibre of infinite length. If $E_f > E_m U$, the condition of simultaneous breaking will be satisfied for a fibre of finite length. However, $E_f < E_m U$ represents the "forbidden region", where the condition of simultaneous breaking can never be reached. One can imagine the case of $E_f = E_m$, with $U_f > U_m$. While the stress and energy level is the same everywhere, the matrix will always break first because it possesses a smaller cohesive energy. The occurrence of the divergence in the critical aspect ratio at low elastic modulus ratio has significance for the prediction of this quantity in metal and ceramic matrix composites. In these materials the critical aspect ratio is usually estimated as [4, 5] $S_c \propto \sigma_f^*/\tau_m^*$ where σ_f^* is the breaking stress of the fibre and τ_m^* is usually related to the yield stress for a metal matrix and to the interfacial strength for a ceramic matrix. As discussed above, the conventional approach neglects the change in loading efficiency as the elastic modulus of the fibre is varied. The loading efficiency decreases as the elastic modulus of the fibre approaches the matrix, resulting in an increase in the fibre length needed to achieve maximum stress transfer. While the results of this paper concern elastic/brittle materials only, it is nevertheless expected that because ceramic fibres and matrices have moduli in the range of 500 GPa and higher [28, 29], and metal matrices have moduli in the range of 150 GPa [31], the critical aspect ratio for these composites will be larger than the classical estimate.

The results of this work, namely that the divergence of the aspect ratio for low value of E is followed by a minimum whose location is a function of the ratio of the cohesive energies, could possibly account for the scatter of the data reported by Asloun *et al.* [18]. If, in fact, critical aspect ratio is indeed a function of the ratio of cohesive energies as well as of the ratio of elastic moduli, this extra parameter can account for the difference between thermosets/thermoplastics and elastomeric matrices found by Asloun *et al.* (see Fig. 2). Elastomeric matrices are known to be tougher than thermosetting or thermoplastic matrices [32]. Fig. 4b clearly indicates that the critical length decreases with a decreasing value of the ratio of cohesive energies of the fibre and the matrix, U. Furthermore, this extra parameter also suggests that it may not always be appropriate to compare one experimental system to another as was done in the work of Asloun *et al.*

The results of Asloun *et al.* indicate that the critical lengths measured vary as $E^{1/2}$ for E large, in disagreement with Termonia [16, 17] and this work, where the critical length varies as E. The difference can be explained by the fact that our model and Termonia's assume a perfect elastic regime. In an experimental situation, the stress concentration might not be as high as it would be for a matrix with perfect elastic behaviour due to viscoelastic interactions (creep) or plasticity. Hence future work will study in particular the effect of viscoelastic interactions on the critical aspect ratio before undertaking the study of multifibre systems with interface characteristics.

Acknowledgements

The authors thank M. Luton, D. Srolovitz, J. P. Dismukes and J. Hwang for useful discussions and comments.

References

1. A. KELLY and G. J. DAVIES, *Metall. Rev.* **10** (1965) 37.
2. G. S. HOLISTER and C. THOMAS, "Fibre Reinforced Materials" (Elsevier, London, 1966) p. 16.
3. B. W. ROSEN and N. F. DOW, in "Fracture", Vol. 7, edited by H. Leibowitz (Academic, New York, 1972) p. 1.
4. M. R. PIGGOTT, in "Load Bearing Fibre Composites" (Pergamon, Oxford, 1980) p. 83.
5. D. HULL, "An Introduction to Composite Materials" (Cambridge University Press, Cambridge, 1981) p. 142.
6. H. L. COX, *Brit. J. Appl. Phys.* **3** (1952) 72.
7. A. S. CARRARA and E. J. McGARRY, *J. Compos. Mat.* **2** (1968) 222.
8. R. A. LARDER and C. W. BEADLE, *ibid.* **10** (1976) 21.
9. E. D. REEDY, *ibid.* **18** (1984) 595.
10. S. R. NUTT and A. NEEDLEMAN, *Scripta Metall.* **21** (1987) 705.
11. W. R. TYSON and G. J. DAVIES, *Brit. J. Appl. Phys.* **16** (1965) 199.
12. D. M. SCHUSTER and E. SCALA, *Trans. Met. Soc. AIME* **230** (1965) 1491.
13. B. W. ROSEN, *AIAA J.* **2** (1964) 1985.
14. *Idem*, "Fiber Composite Materials" (ASM, Metals Park, OH, 1965) p. 1.
15. C. GALIOTIS, R. J. YOUNG, P. H. J. HEUNG and D. N. BATCHELDER, *J. Mater. Sci.* **19** (1984) 3640.
16. Y. TERMONIA, *ibid.* **22** (1987) 504.
17. *Idem, ibid.* **22** (1987) 1733.
18. E. M. ASLOUN, M. NARDIN and J. SCHULTZ, *ibid.* **24** (1989) 1835.
19. A. KELLY and W. R. V. TYSON, *Mech. Phys. Solids* **13** (1965) 329.
20. M. J. FOLKES and W. K. WONG, *Polymer* **28** (1987) 1309.
21. W. D. BASCOM and R. M. JENSEN, *J. Adhesion* **19** (1986) 219.

22. P. D. BEALE and D. J. SROLOVITZ, *Phys. Rev. B* **37** (1988) 5500.
23. W. H. YANG, D. J. SROLOVITZ, G. N. HASSOLD and M. P. ANDERSON, in "Simulation and Theory of Evolving Microstructures", edited by M. P. Anderson and A. D. Rollett (TMS, Warrendale, PA, 1990) p. 277.
24. W. H. YANG, unpublished (1989).
25. G. N. HASSOLD and D. J. SROLOVITZ, *Phys. Rev. B* **39** (1989) 9273.
26. Y. TERMONIA, *J. Mater. Sci.* **25** (1990) 4644.
27. M. R. PIGGOTT, *Compos. Sci. Tech.* **30** (1987) 295.
28. "Engineering Property Data on Selected Ceramics", Vols 1–3, edited by J. F. Lynch (Metals and Ceramics Information Center, Columbus, OH, 1981).
29. "Handbook of Materials Science", Vol. 3, edited by C. T. Lynch (CRC Press, Boca Raton, Florida, 1975).
30. T. W. CLYNE, *Mater. Sci. Engng* **A122** (1989) 183.
31. C. R. BARRETT, W. D. NIX and A. S. TETELMAN, "The Principles of Engineering Materials" (Prentice-Hall, Englewood, NJ, 1973) p. 540.
32. F. W. BILLMEYER Jr, "Textbook of Polymer Science" (Wiley, New York, London, Sydney, Toronto, 1971) p. 185.
33. H. SIMON, PhD thesis, Université de Haute-Alsace, Mulhouse, France (1984).
34. H. SIMON, F. BOMO and J. SCHULTZ, in "Proceedings of the European Plastics Conference", Paris, France, Vol. IV(9) (1982) pp. 1–5.
35. J. SCHULTZ, L. LAVIELLE and C. MARTIN, *J. Adhesion* **23** (1987) 45.
36. T. OHSAWA, A. NAKAYAMA, M. MIWA and A. HASEGAWA, *J. Appl. Polym. Sci.* **22** (1978) 3203.
37. J. M. ROBINSON, R. J. YOUNG, C. GALIOTIS and D. N. BATCHELDER, *J. Mater. Sci.* **22** (1987) 3642.
38. J. SCHULTZ, L. LAVIELLE and H. SIMON, in "Proceedings of the International Symposium on Science and New Applications of Carbon Fibres", Toyohashi, Japan, November 1984 (Toyohashi University of Technology, Japan, 1984) p. 125.
39. G. GUILPAIN and J. B. DONNET, personal communications (1987).
40. L. T. DRZAL, M. J. RICH, M. F. KOENIG and P. F. LLOYD, *J. Adhesion* **16** (1983) 133.
41. L. ONGCHIN, W. K. OLENDER and F. H. ANCKER, in "Proceedings of the 27th Annual Technical Conference", SPI/ Reinforced Plastics – Composite Institute, Washington (1972) Section 11-A.
42. M. XIE, PhD thesis, Institut National des Sciences Appliquées, Lyon, France (1987).
43. M. J. FOLKES and W. K. WONG, *Polymer* **28** (1987) 1309.
44. F. BOMO, PhD thesis, Université de Haute-Alsace, Mulhouse, France (1983).

Received 12 April
and accepted 19 July 1991